Research Article

Awali Priyono*, Rexha Verdhora Ry, Andri Dian Nugraha, Aditya Lesmana, Billy S. Prabowo, Yayan M. Husni, A. Ardianto, Nyoman Witarsa, and Buyung I. Sutan

On the use of low-frequency passive seismic as a direct hydrocarbon indicator: A case study at Banyubang oil field, Indonesia

https://doi.org/10.1515/geo-2022-0587 received May 31, 2023; accepted November 22, 2023

Abstract: Low-frequency passive seismic (LFPS), discussed in recent years, has emphasized a strong correlation between the spectral properties and the presence of hydrocarbon reservoirs. While the theoretical background supporting this phenomenon is still debated, its application has been popular in Indonesia and exposes broad possibilities for exploration. In this study, we conducted a survey at an oil field in Central Java, Indonesia, investigating the case of using this technique as a direct hydrocarbon indicator (DHI). In spatial and temporal measurements, we examined the hydrocarbon-related energy above the reservoir boundary based on several attributes of passive seismic recordings: polarization, power spectral density (PSD), and vertical-to-horizontal spectral ratio (VHSR). We address some issues: (1) the anomalies are not always vertically polarized, so the use of VHSR is unlikely to be reliable; and (2) the anomalies are getting amplified during days, so in anomalies mapping, normalizing the amplification requires calibration. Regardless, LFPS is still applicable in quantifying hydrocarbon-related energy. We recommend using PSD as a primary spectral attribute for DHI. In addition, it is also critical to synchronize the measurements at different sites to obtain an unbiased quantification of hydrocarbon-related energy.

Keywords: passive seismic, DHI, spectral anomalies

1 Introduction

The use of low-frequency passive seismic (LFPS) as a direct hydrocarbon indicator (DHI) has been proposed according to several empirical studies [1–5]. These studies conclude by finding a consistent phenomenon showing a strong correlation between spectral properties and the presence of hydrocarbon reservoirs. The so-called hydrocarbon-related spectral anomalies can be observed on passive seismic recordings between 1 and 6 Hz frequencies, with a peak around 3 Hz. The anomalies become strong above reservoirs, decrease toward the rims, and are entirely absent in non-reservoir areas.

In contrast, a growing number of case studies have doubted the applicability of this technique as an indicator of hydrocarbon presence [6–10]. They show that the observed anomalies are not related to the presence of hydrocarbons. Instead, anthropogenic noises such as production facilities and traffic greatly influence the so-called anomalies. Studies also propose that the spectral anomalies may relate to Rayleigh wave distortions above the reservoir due to anticline structure [11,12].

Despite this lively debate in academics, most oil and gas industries in Indonesia have been calling for applications of LFPS surveys. Due to its practicality and low cost, LFPS has become popular and widely used in exploration, granted by industries. Accordingly, the Indonesian government recommends this technique be applied in exploration and field development, and it also greatly influences the decision of a well-drilling location. Some have reported its success stories (e.g., [13–17]). For instance, Haris et al. [16] improved the analyses by applying time reverse modeling to identify the source of the spectral anomalies, and

Rexha Verdhora Ry, Andri Dian Nugraha: Global Geophysics Group, Faculty of Mining and Petroleum Engineering, Institut Teknologi Bandung, Ganesha 10, Bandung 40132, Indonesia

Aditya Lesmana, Billy S. Prabowo, Yayan M. Husni, A. Ardianto: Geothermal and Volcanology Laboratory, Faculty of Mining and Petroleum Engineering, Institut Teknologi Bandung, Ganesha 10, Bandung 40132, Indonesia

Nyoman Witarsa: Geological Engineering, Universitas Pakuan, Bogor, Indonesia

Buyung I. Sutan: Banyubang Blora Energy (BBE), Blora, Indonesia

^{*} Corresponding author: Awali Priyono, Global Geophysics Group, Faculty of Mining and Petroleum Engineering, Institut Teknologi Bandung, Ganesha 10, Bandung 40132, Indonesia, e-mail: priyonoawali@gmail.com, awali@itb.ac.id

2 — Awali Priyono et al. DE GRUYTER

Sudarmaji et al. [17] denote the observation of a spectral ratio peak in a poroelastic reservoir based on 2D seismic wave propagation. In addition, passive seismic study of ambient noise has been successively utilized to delineate sediment layers in basins [18,19].

Motivated by the possibility of using LFPS to quantify hydrocarbon-related energy, we undertook a passive seismic survey at the Banyubang oil field in Central Java, Indonesia. Acting as a case study and test site, we investigated the correlation between the spectral properties and the reservoir location in spatial and temporal measurements. An array geometry consisting of seven seismometers was deployed to record the data of velocity ground motions. Concerning the spectral attributes, we analyze power spectral density (PSD) and vertical-to-horizontal spectral ratio (VHSR) proposed by Lambert et al. [4] and Saenger et al. [5]. We investigated their spatial variations as DHI above the known reservoir boundary and their anomalies along with time. We also analyze their polarization to estimate wave directions.

This empirical study shows the linear relationship between the power spectra density - the integral of the Z-component (PSD-IZ) value in a frequency range of 1–4 Hz and the indication of a hydrocarbon reservoir in spatial,

but not so much for VHSR in this case. Meanwhile, for temporal variations, their hydrocarbon-related anomalies keep emerging continuously over time in days and nights. However, significant amplifications on vertical PSD have been observed during days. Following this investigation, we denote further recommendations for LFPS surveys, such as synchronized measurements to normalize the amplitude of spectral attributes.

2 Data

2.1 Geology of the Banyubang field

Banyubang oil field is located in Central Java, Indonesia, about 120 km east of Semarang City. Geologically, the field lies in the North-East Java Basin area [20,21]. Regional tectonic developments in the North-East Java Basin result from interactions between three continental plates: the Australian plate in the south, the Eurasian plate in the north, and the Pacific oceanic plate in the west. The developing structural pattern generally has a relative west–east

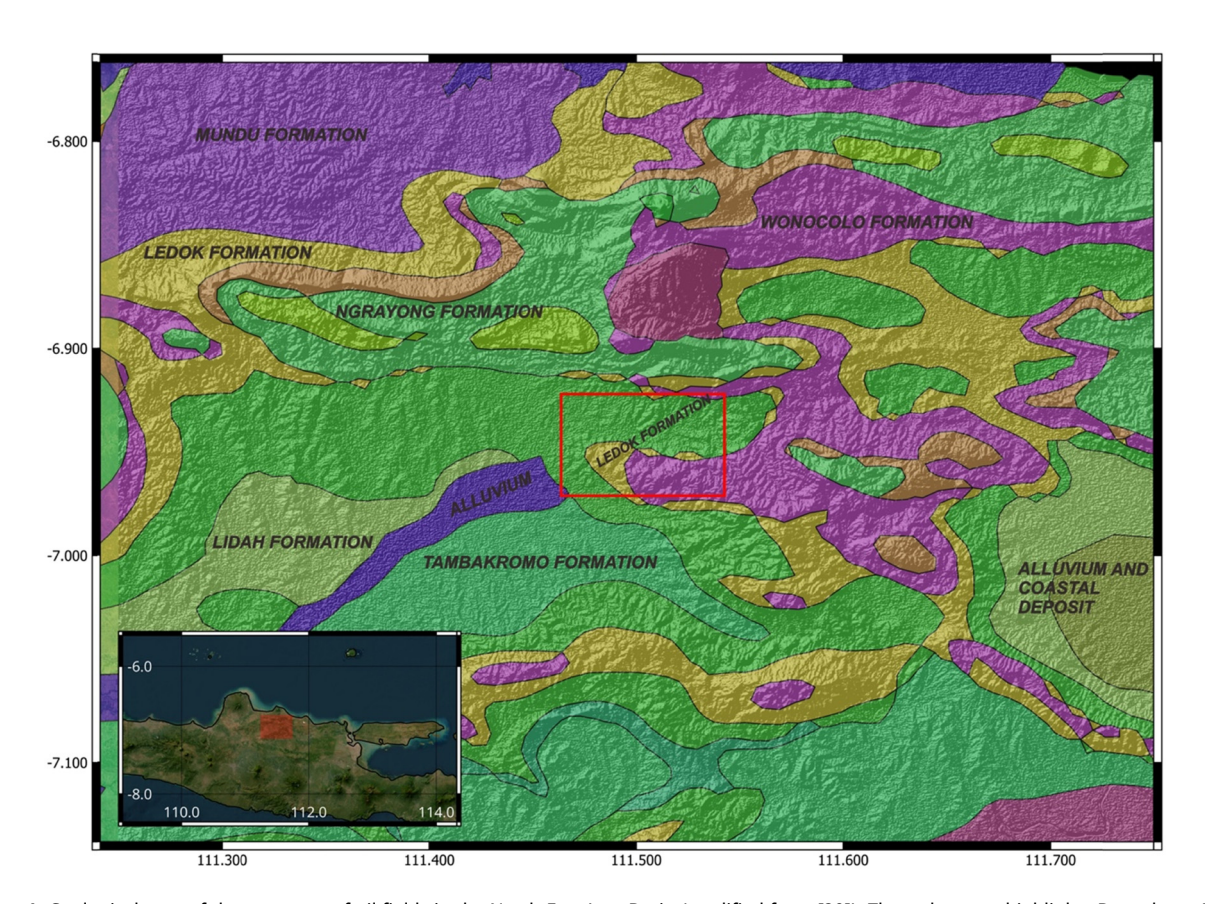


Figure 1: Geological map of the west part of oil fields in the North-East Java Basin (modified from [20]). The red square highlights Banyubang Field.

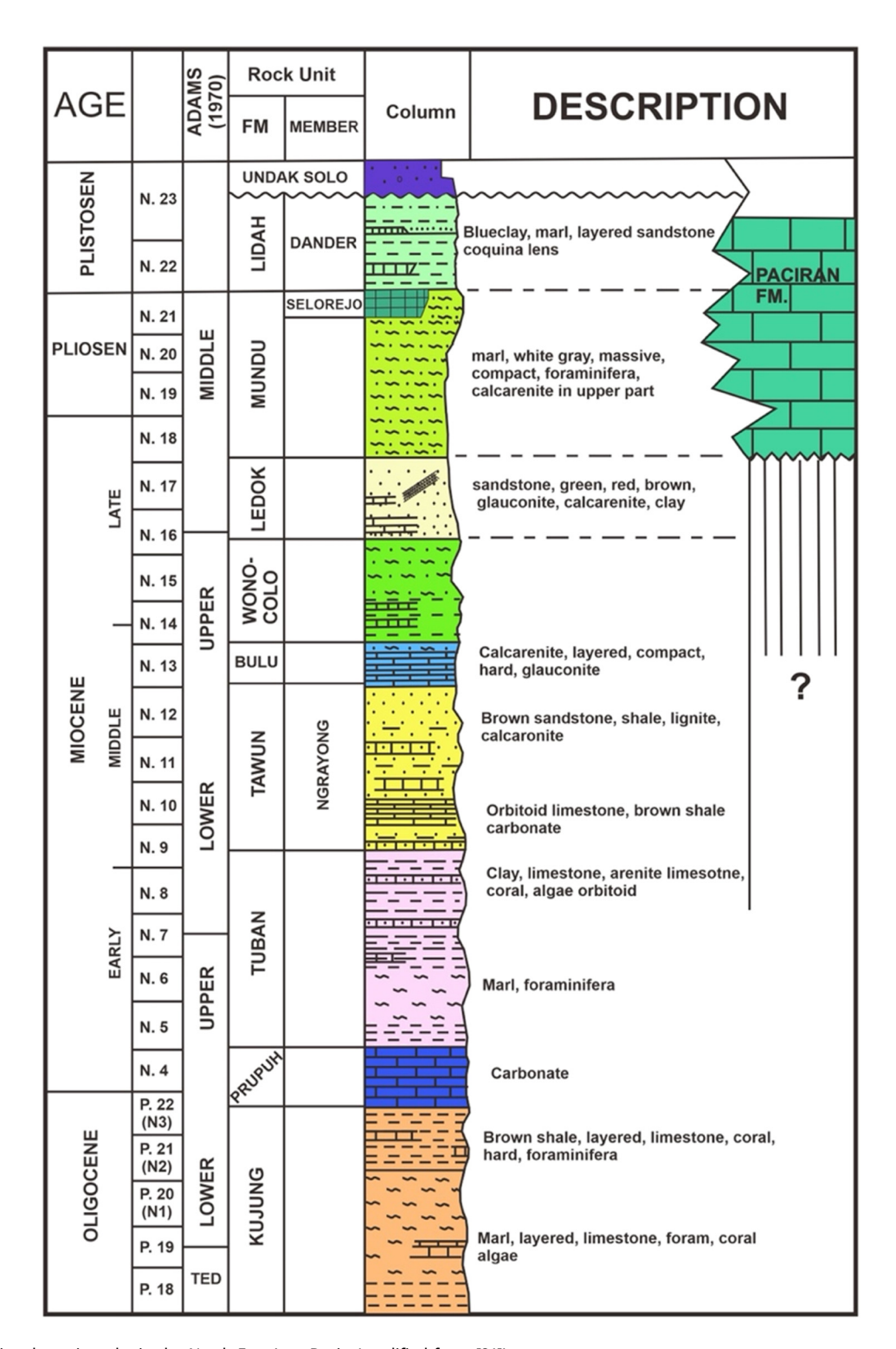


Figure 2: Regional stratigraphy in the North-East Java Basin (modified from [21]).

orientation, including the Kendeng (Kendeng zone) anticlinorium in the south and the Rembang (Rembang zone) anticlinorium in the north. In between is separated by Randublatung depression.

Banyubang Field (Figure 1) is an old oil field that was discovered in 1903, and by 1933, more than 35 wells had been drilled. However, this field was abandoned in 1933 after reaching a cumulative of 590,000 barrels of oil. The main object of the reservoir is the clastic limestone layer of the Middle Miocene Ngrayong Formation. The stratigraphy of the North-East Java Basin is shown in Figure 2. The Banyubang Field has three structures, each in the west, east, and south. Drilling wells are primarily located in the eastern structure, reaching 33 old Dutch wells. Meanwhile, after 2010, four new wells were drilled in the western structure (we noted one of them as Well-B).

The main oil producer in the west structure is limestone facies. Ngrayong formation at a depth of 510–560 m, with 25–29% porosity and a water saturation of 31–45%. In a 720–750 m depth, the reservoir consists of limestone facies, Ngrayong Formation with porosity of 24–28%, and water saturation of 50–60%.

2.2 Data acquisition

The LFPS survey was conducted between 13 and 15 July 2018 on Banyubang Field. Three-component (3C) broadband seismometers (Figure 3a) were deployed in an array geometry (Figure 3b) and designed to observe hydrocarbon-related energy in spatial and temporal measurements. The geometry of the survey consists of an array (line A) with seven stations deployed simultaneously and an additional point (station C5) placed outside the array at different times. Line A extends from North to South with a proven well of oil reservoir as a center (Well-B). The space

between stations is around 250 m, and the measurements were conducted for 48 h continuously during days and nights. Meanwhile, the additional station C5 was only set for 2 h.

We used Geobit borehole seismometers to record velocity ground motions with a sample rate of 100 Hz. The seismometers have a flat frequency response from 10 s to 98 Hz with a high sensitivity of 1,500 V/m/s. Where possible, the sensors were covered and buried up to 0.5 m deep for firm ground contact and to minimize surface noise. In addition, each sensor was equipped with an internal 32-bit digitizer (Geobit SRi32L) as a logger and an external global positioning system receiver to allow precise time synchronization of the measurements. Figure 3(a) shows a portable broadband seismometer and setup in a field.

When installing a borehole seismometer, we used a compass to show the north and a water pass to ensure the sensor was perpendicular to the bottom of the hole. We put the battery and digitizer in a plastic box for security reasons. The box was wrapped using a trash bag and buried at a depth of 50 cm near the borehole seismometer. The same treatment is given for all stations.

3 Data processing

A single seismometer continuously recorded velocity ground motions for at least 48 h during days and nights. We analyzed

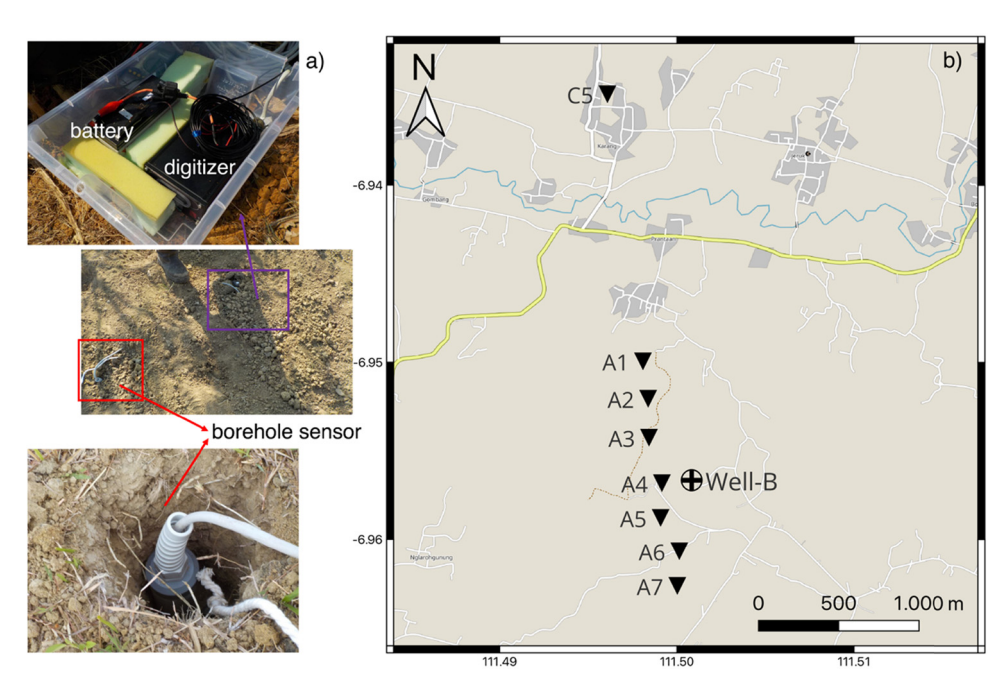


Figure 3: (a) Set-up of borehole broadband seismometer in the field. (b) Acquisition layout of LFPS survey: Line A consisted of seven stations and an additional station C5. The black triangles are stations, and the crossed circle is Well-B.

the data in time and frequency domains to quantify hydrocarbon-related anomalies beneath every station. The data processing was summarized based on the proposed approach to using the spectral properties of the ground motions as a DHI [4,5]. First, the time series of clean signals was selected and windowed. Then, the signals were analyzed in the frequency domain to calculate PSD and vertical-to-horizontal

(V/H) spectral ratio for every station, respectively. In addition,

we analyzed their polarizations to observe wave directions.

3.1 Data selection

DE GRUYTER

The raw data in the time domain recorded hydrocarbonrelated signals and artificial interferences. The first step in data processing was to select a data window free from any transient noise signature. This aims to keep clean signals for calculating spectral attributes, represented by several data intervals to get stacked later.

This study uses an interval of 80 s in data windowing. Figure 4 gives an example of this data selection; every colored window represents the clean signals used in further processing steps. Meanwhile, the other windows contain apparent artificial noise signatures, which were eliminated. Although this example only shows 20 min of data, we used all recorded 48 h for data processing. Many data windows are computed to strengthen hydrocarbonrelated anomalies.

3.2 Polarization

Principal component analysis of particle motion as a function [22] is beneficial in this study to give information on the incoming wave directions [23,24] and their variations in time. For example, on a signal related to a hydrocarbon reservoir, the incoming waves are expected to come predominantly from below the subsurface, represented by dip and azimuth.

The first step in our polarization procedure is to bandpass filter the 3-C data in the time domain. We use a bandpass filter between 1.5 and 4 Hz. Then, we followed the calculation described by Saenger et al. [5] as polarization analysis. In short, the dip and azimuth are derived from the orientation of the largest eigenvector p_1 , for each component of east-west ($H_{\rm EW}$), north-south ($H_{\rm NS}$), and vertical (V). The dip φ and azimuth θ are calculated as follows:

$$\varphi = \tan^{-1} \frac{p_1(V)\sqrt{2}}{\sqrt{p_1(H_{\rm EW})^2 + p_1(H_{\rm NS})^2}},$$
 (1)

$$\theta = \tan^{-1} \frac{p_1(H_{\rm NS})}{p_1(H_{\rm EW})}.$$
 (2)

Dip φ is 0° for horizontal polarization and goes to 90° along with a positive vertical axis. Azimuth θ is measured counterclockwise from the north. As an example, Figure 5 shows the time variations of dip φ , azimuth θ , and rectilinearity [5] by analyzing 80-s time intervals for station A2 data.

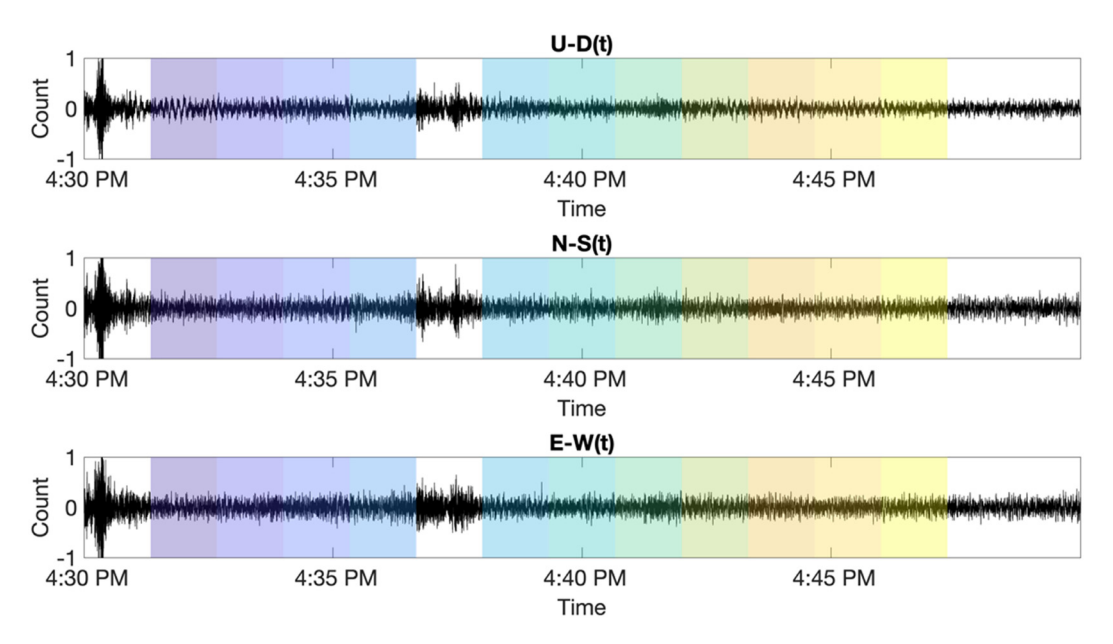


Figure 4: Time series of raw velocity ground motions for the vertical, north-south, and east-west components, respectively. Every colored window (except the black ones) is an 80-s interval of clean signals.

6 — Awali Priyono et al. DE GRUYTER

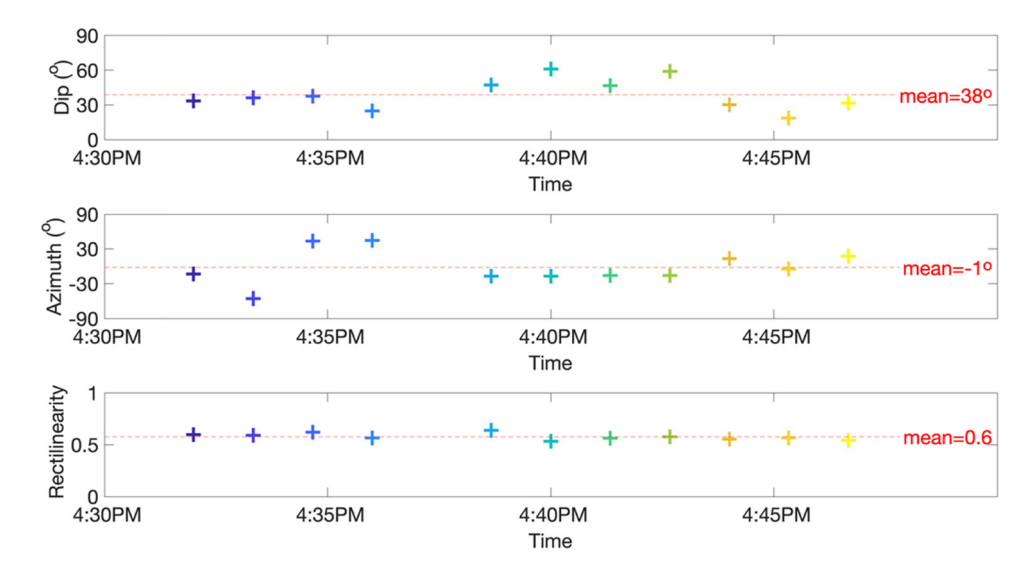


Figure 5: Polarization attributes of dip and azimuth for every colored window in Figure 4 and their mean value (red dashed line). In addition, rectilinearity measures how linearly the incoming wavefield is polarized.

3.3 PSD

The earlier studies [1,2] quantified hydrocarbon-related spectral anomalies by extracting the peak amplitude of PSD at the vertical component between 2 and 4 Hz frequencies. They emphasize the linear relationship between the PSD value and the high indication of a hydrocarbon reservoir beneath the observing station. This technique is then complemented [4,5] by using integration along with a hydrocarbon-related frequency range. This completion, so-called by PSD-IZ may better quantify the energy of spectral anomalies.

Figure 6 depicts the calculation of PSD-IZ. First, the PSD spectra for all windows were stacked to strengthen the signal (Figure 6a), and then, an averaged PSD spectrum

(Figure 6b) was obtained. Second, the minimum amplitude between 1 and 1.5 Hz was selected individually from the average PSD spectrum to consider noise floor variations. Finally, the integral of spectral amplitudes above the noise level defines the value of PSD-IZ.

The frequency interval of the integrated spectra must lie between the ocean wave peak and the anthropogenic noise peak [2,5]. Hence, the frequency interval may vary depending on the survey background. For references, Lambert et al. [4] used the interval of 1–5 Hz in their study, while Saenger et al. [5] preferred to calculate PSD-IZ from 1 to 3.7 Hz. In this study, we used a frequency interval of 1–4 Hz. Accordingly, we used PSD-IZ to quantify hydrocarbon-related spectral anomalies rather than restricting them to peak strength at specific frequencies.

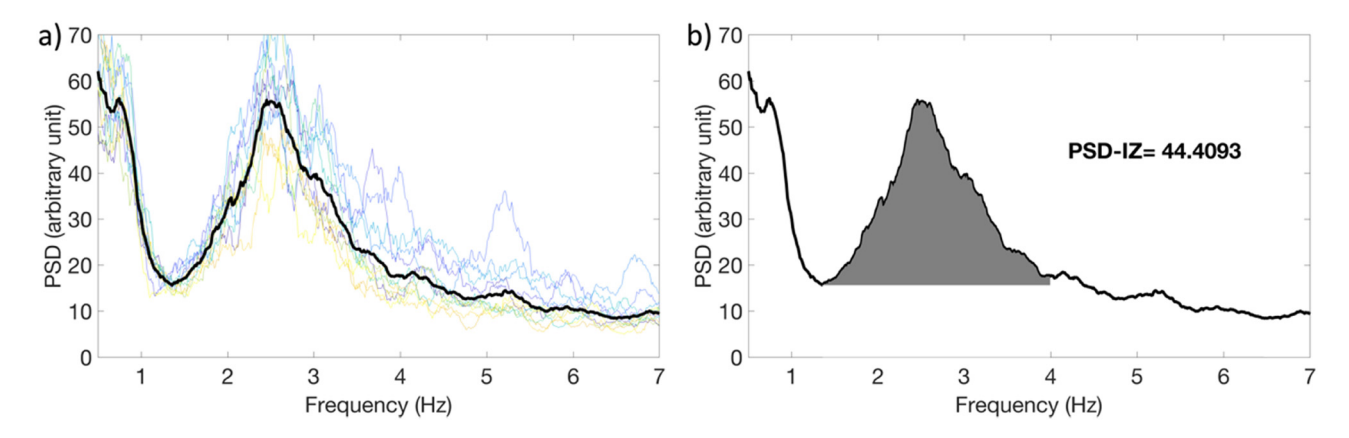


Figure 6: (a) Spectral attribute of PSD calculated from 11 windows. Each colored line represents the spectra from colored windows in Figure 4, respectively, while the black line is the mean value. (b) Averaged PSD spectrum with its integral area (gray) calculating PSD-IZ from 1 to 4 Hz by considering noise level.

3.4 VHSR

Lambert et al. [4] and Saenger et al. [5] introduced another independent guidance to quantify hydrocarbon-related spectral anomalies: VHSR. This spectral ratio normalizes spectra at the vertical component against the horizontal component. Assuming that waves propagate vertically from below and Pwaves resonance is dominant, the energy of anomalies would be higher on the vertical component. Therefore, VHSR related to hydrocarbon indication has a value over 1. Compared to PSD-IZ, this quantification is more stable in time and may give fair compensation to surface rock properties in measurements [4,5].

The spectral amplitudes at the horizontal component, H(f), can be determined by quadratic averaging the spectral amplitudes at both the east-west component $H_{EW}(f)$ and the north-south component $H_{NS}(f)$ as follows:

$$H(f) = \sqrt{\frac{1}{2}(H_{\text{EW}}(f)^2 + H_{\text{NS}}(f)^2)}.$$
 (3)

Then, where V(f) is the spectral amplitude at the vertical component, VHSR is given as follows:

$$V/H(f) = \frac{V(f)}{H(f)} \tag{4}$$

Figure 7 illustrates the determination of VHSR. First, the spectral ratios are obtained for every window using equations (3) and (4). Then, they are stacked to obtain an averaged VHSR, like what has been done in calculating PSD. A maximum VHSR is determined between 1 and 5 Hz frequencies (V/H max). Therefore, hydrocarbon-related energy should make its value lie above 1 [5].

Results and discussion

4.1 Hydrocarbon-related anomalies

PSD-IZ and VHSR have been described in the previous section as tools to quantify the energy of hydrocarbon-related anomalies. We used synchronized records of seven seismometers at Line A above a known hydrocarbon reservoir. The depth profile beneath this area (Figure 8) has been obtained using a seismic reflection study [25] and existing Well-B that the anticline structure confines the reservoir. Line A focused on the reservoir boundary to observe the spatial variation of the anomalies. Meanwhile, station C5 is located far away and out from the reservoir.

According to the log data obtained in Well-B, the oil is reserved in the Ngrayong formation (limestone) at 508-560 m, with 28–29% porosity. The reservoir is between LC and L1 (Figure 8) and has ~20% oil content and 30-44% water saturation. Station A4 is the nearest observation to this Well-B.

Figure 9 shows the result regarding the spectral anomalies above the hydrocarbon reservoir. A PSD amplitude anomaly between 2 and 3 Hz is clearly observed above this reservoir area as a promising DHI. Compared to C5, its PSD is considered small. The strongest anomalies of the PSD-IZs are found at stations A2, A3, and A7, and they are not necessarily related to the thickness of the reservoir beneath them. These anomalies may also be controlled by the porosity percentage varying in spatial. However, we emphasize the linear relationship between the PSD-IZ value and the high indication of a hydrocarbon reservoir, which these seven stations present well.

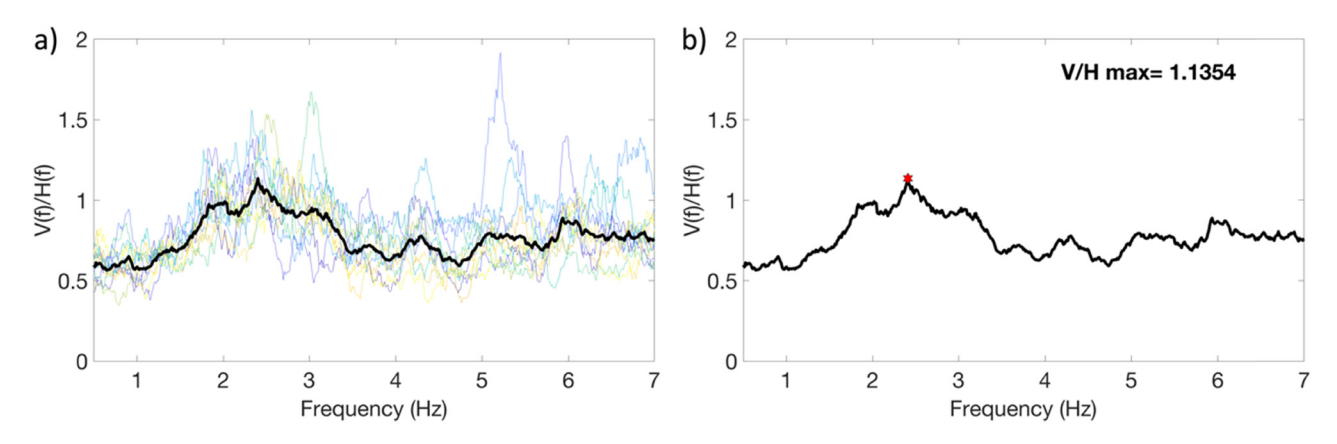


Figure 7: (a) VHSR from several windows. Every colored line represents VHSR from colored windows in Figure 3, respectively, while the black line is their average. (b) Averaged VHSR and its maximum (red star) between 1 and 5 Hz.

8 — Awali Priyono et al. DE GRUYTER

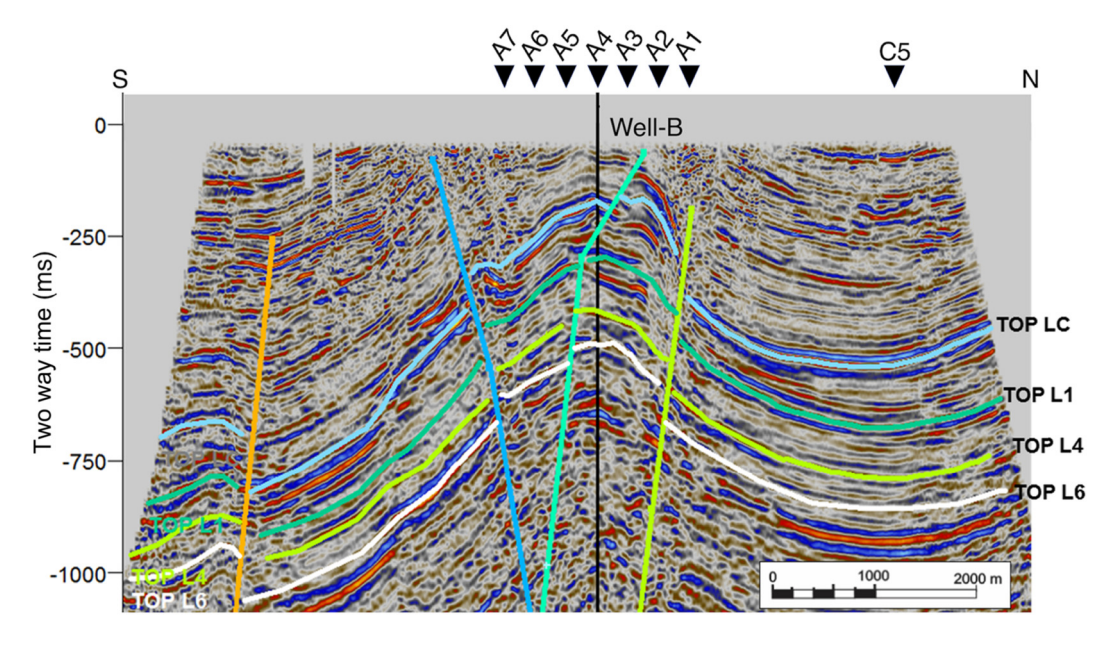


Figure 8: Profile of seismic reflection parallel to Line A, modified from [25]. LC, L1, L4, and L6 represent designated layers. The black triangles represent stations.

Meanwhile, a more complex pattern is shown for VHSR. First, their maximum VHSRs (*V/H* max) are mainly near to or below 1. The assumption of the dominance of vertical P-wave resonance [4,5] is not proven here. The contradictive suggestion regarding this has been proposed by Vesnaver et al. [26] that ray paths through an anticline structure should not be vertically polarized. It may be true in this study, causing the VHSR to get damped and decrease. Later, we observe it deeper by analyzing their polarizations.

Second, it can be observed that the VHSR gets more potent at the edge of the anticline structure rather than being the strongest at the anticline peak (beneath A4). While it can also be related to the higher hydrocarbon indication, for instance, at A2 and A7, the pattern is inconsistent for all stations. We suggest that the seismic properties of shallow sediment layers shade the hydrocarbon-related energy and that a lower VHSR represents the seismic velocity contrast in this area [27]. This may be because the lower VHSR represents the thicker sediment layer, and when the layer gets thinner, it strengthens the VHSR. In addition, their inconsistency could be influenced by the scattered effect caused by the geometry of the anticline.

A similar signature of VHSR is also reported by Ali et al. [6,8–10] and Hanssen [7]. The topography, shallow seismic properties, and other near-surface characteristics may greatly influence VHSR. Even in a low-noise environment, a random low energy from anywhere can induce a significant value of VHSR [7]. Moreover, near-surface

geological rocks can give a particular anomaly to spectral ratio at specific frequencies depending on their geometry and seismic properties [27]. Therefore, it is highly arguable that VHSR can be used individually as a DHI, such that a higher or lower VHSR does not directly indicate the existence of a hydrocarbon reservoir. However, as a complimentary of PSD-IZ, it is beneficial, for instance, to increase the confidence of interpretations or to estimate the thickness of sediment layers.

4.2 Polarization analyses

Whether the anomalies come directly from beneath the station is still being discussed. Dangel et al. [1] suggested that the spectral anomalies they observed are directly related to the hydrocarbon reservoir beneath the station, meaning that low-frequency seismic waves dominated by P-waves come vertically from below. Lambert et al. [4] and Saenger et al. [5] supported this notion and exposed the use of VHSR in quantifying vertically polarized anomalies. In contrast, Ali et al. [6,8–10] found that the so-called hydrocarbon-related anomalies are dominated by surface waves and greatly influenced by the activities of production wells. Furthermore, as emphasized by Vesnaver et al. [26], ray paths through complex structures (e.g., an anticline) are bent and scattered, so they are not necessarily vertically polarized.

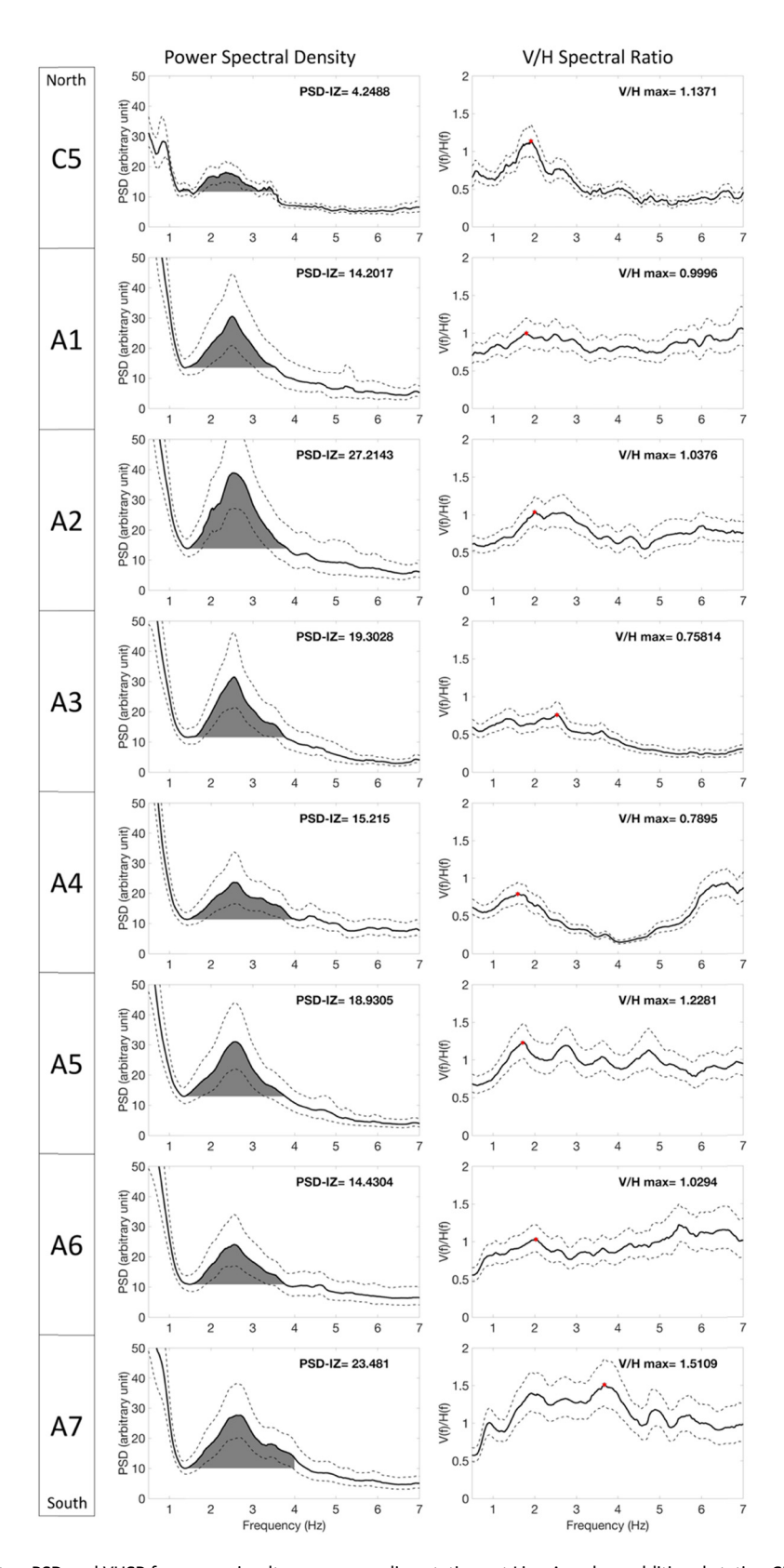


Figure 9: Spectral attributes: PSD and VHSR for seven simultaneous recording stations at Line A and an additional station C5. The bold black lines are the stacked spectra, while the black dashed lines are their standard deviations. Specifically for PSD, the gray areas represent their integral areas in calculating PSD-IZ.

These issues imply that the anomalies observed on stations may not directly relate to the hydrocarbon beneath them. The observed anomalies could also be related to hydrocarbon indication near that site due to scattered waves. Therefore, immediately pointing out DHI on a site that displays hydrocarbon-related anomalies could be deceptive.

We applied polarization analyses on the synchronized records of seven seismometers at Line A, constricting only the hydrocarbon-related frequency band. The pointing arrows shown in Figure 10 depict the particle motions of the dominant waves observed at every station. If the assumption is valid that their particle motions are parallel to their wave directions, such as for P-waves, these arrows may illustrate the principle of incoming waves.

At stations A1, A2, and A7, the dominant waves come from the central part of the array, the hydrocarbon reservoir area. Meanwhile, A3 and A4 are greatly influenced by something not directly coming from below. Finally, it becomes interesting to see stations A5 and A6, which have short vectors of motion, meaning that their waves are mixed by destructive interference of incoming waves from different directions.

Interpreting the anomalies found at A1, A2, and A7 would be fine. They are reliable due to their confirmed source. Their PSD-IZs and VHSR (Figure 9) dominantly come from the hydrocarbon reservoir. Unfortunately, they do not necessarily come vertically from below. The anticline structure in this field made the ray paths of the so-called

low-frequency waves bent and scattered. Figure 10 also illustrates these scattered waves.

4.3 Anomalies continuation

In the practical implementation of LFPS, measuring the data simultaneously for a long recording duration is not necessarily required. Such as, if hydrocarbon-related energy can be measured and observed continuously over time, a single measurement for a sufficient period, e.g., 2–3 h, is applicable in exploration surveys, as suggested by Saenger et al. [5]. This practicality makes the LFPS survey much faster and cheaper, benefiting the oil and gas exploration industries. However, several studies have pointed out the low repeatability of these measurements [7,28]. They reported dissimilar energy of anomalies emerging at different periods of recordings.

That being the case, to observe hydrocarbon-related spectral anomalies over time, we recorded the velocity ground motions data at Line A, located within the reservoir boundary, for 48 h. We used full-duration recordings instead of applying the data selection described in Section 3.1. We undertook a short-time Fourier-transform analysis to calculate the vertical component and VHSR spectrograms. Figure 11 shows the spectrograms of vertical component data for seven stations above the hydrocarbon reservoir area, while Figure 12 shows the spectrograms of VHSR.

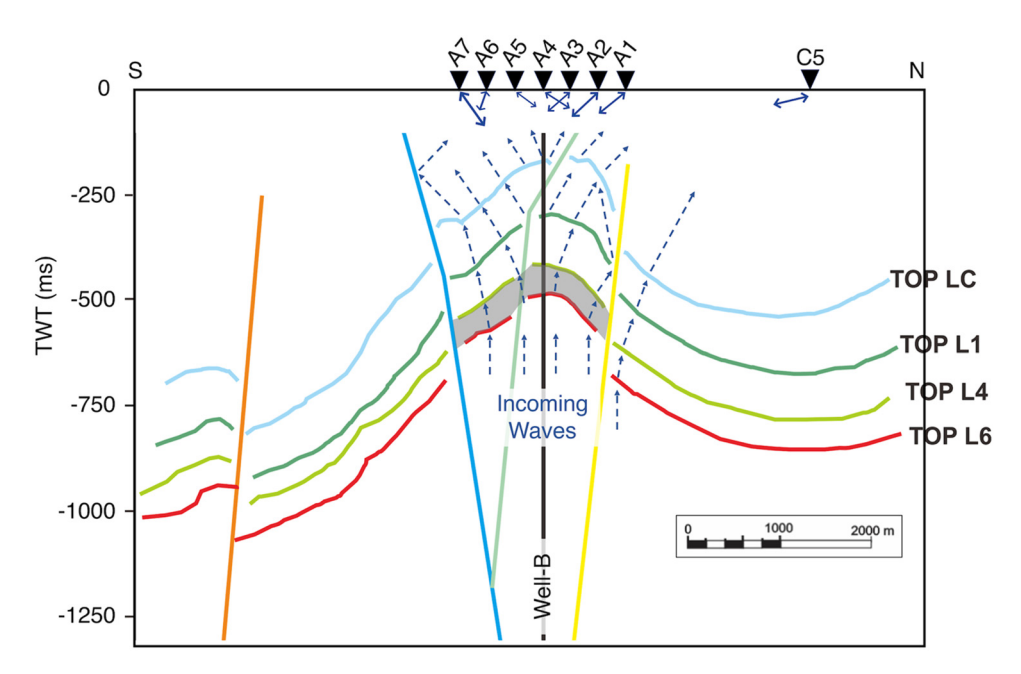


Figure 10: Illustration of the bent and scattered waves through the anticline structure on the south–north profile. The blue arrows depict the dip direction at each station (black triangle) resulting from particle motions of dominant waves in the frequency band of 1.5–4 Hz.

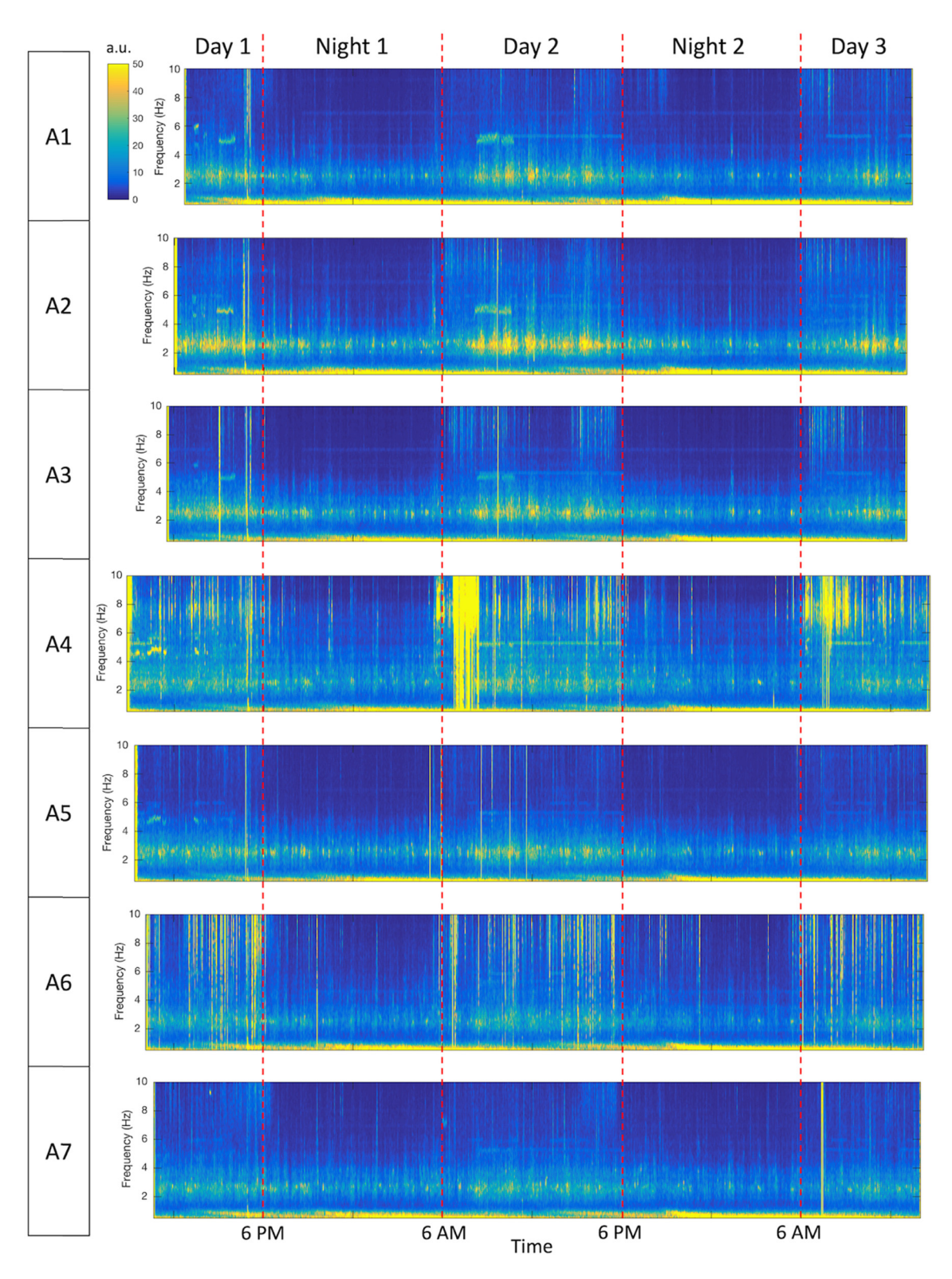


Figure 11: Spectrograms of vertical component data for seven simultaneous recording stations at Line A during days and nights. The color scale represents the amplitudes from 0 to 50 arbitrary units.

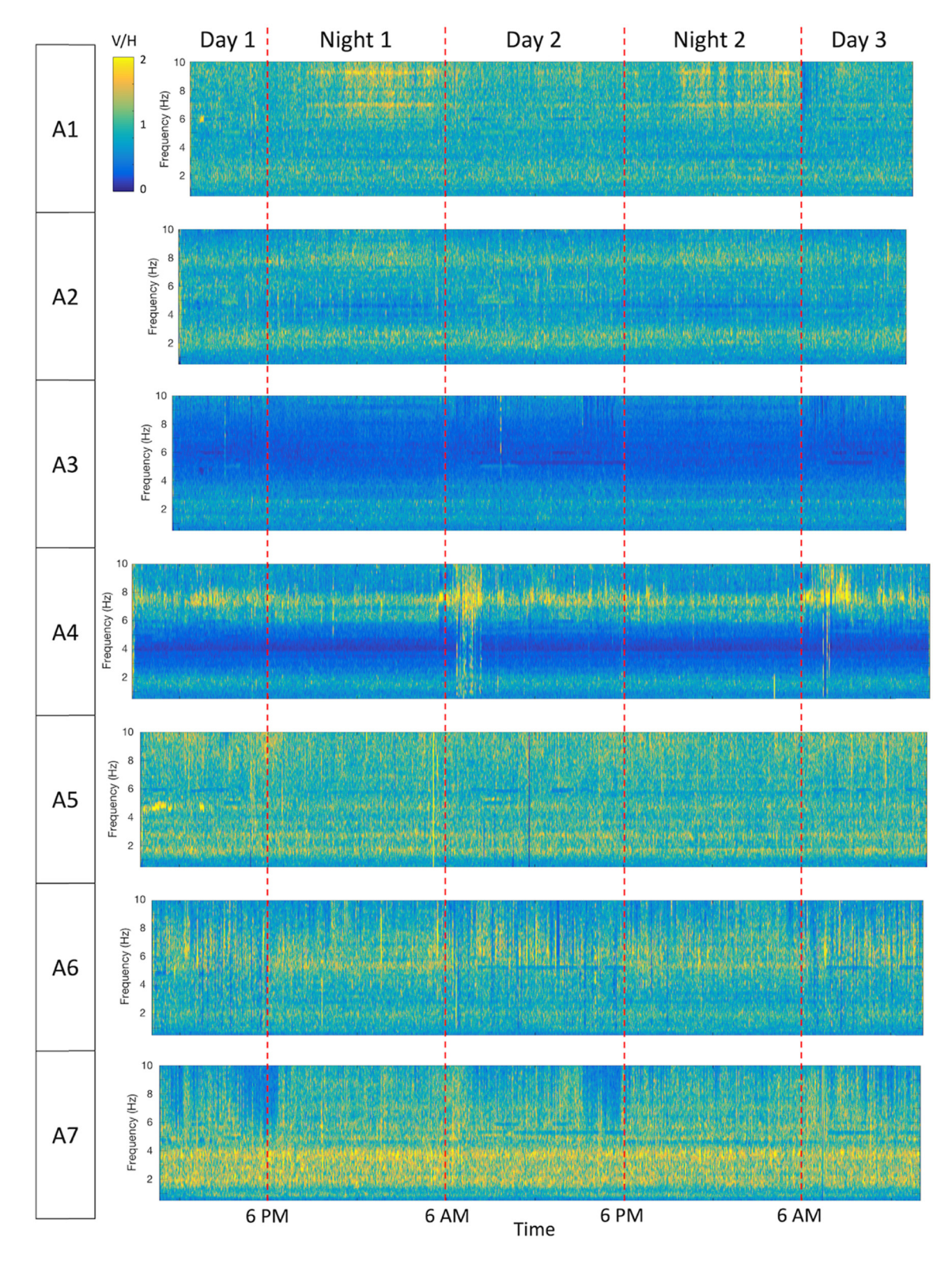


Figure 12: Spectrograms of VHSR for seven simultaneous recording stations at Line A during days and nights. The color scale represents the ratio from 0 to 2.

Blatant artificial interferences are observed in the vertical component at several stations, especially during days (Figure 11). For instance, station A4 records a potent interference on day 2, extending from 0 to 10 Hz and over. This noise influences its recording with a broad frequency width and interrupts the hydrocarbon-related anomalies around 3 Hz. It may lead to misinterpretation of hydrocarbon indications. However, the transient noises are primarily temporal, so they can be removed in the time domain. The windows selection described in Section 3.1 is

crucial to ensure that our results are clean from any misleading disturbance.

Observing hydrocarbon-related energy represented in the vertical spectrograms (Figure 11), strong amplitudes around 3 Hz emerge continuously over time during days and nights. There is no continuous signature at other frequencies; even any different strong amplitude found is temporal. Therefore, it is true that the anomalies can be measured time after time.

However, it should be noted that the anomalies are strengthened during days. A possibility that artificial

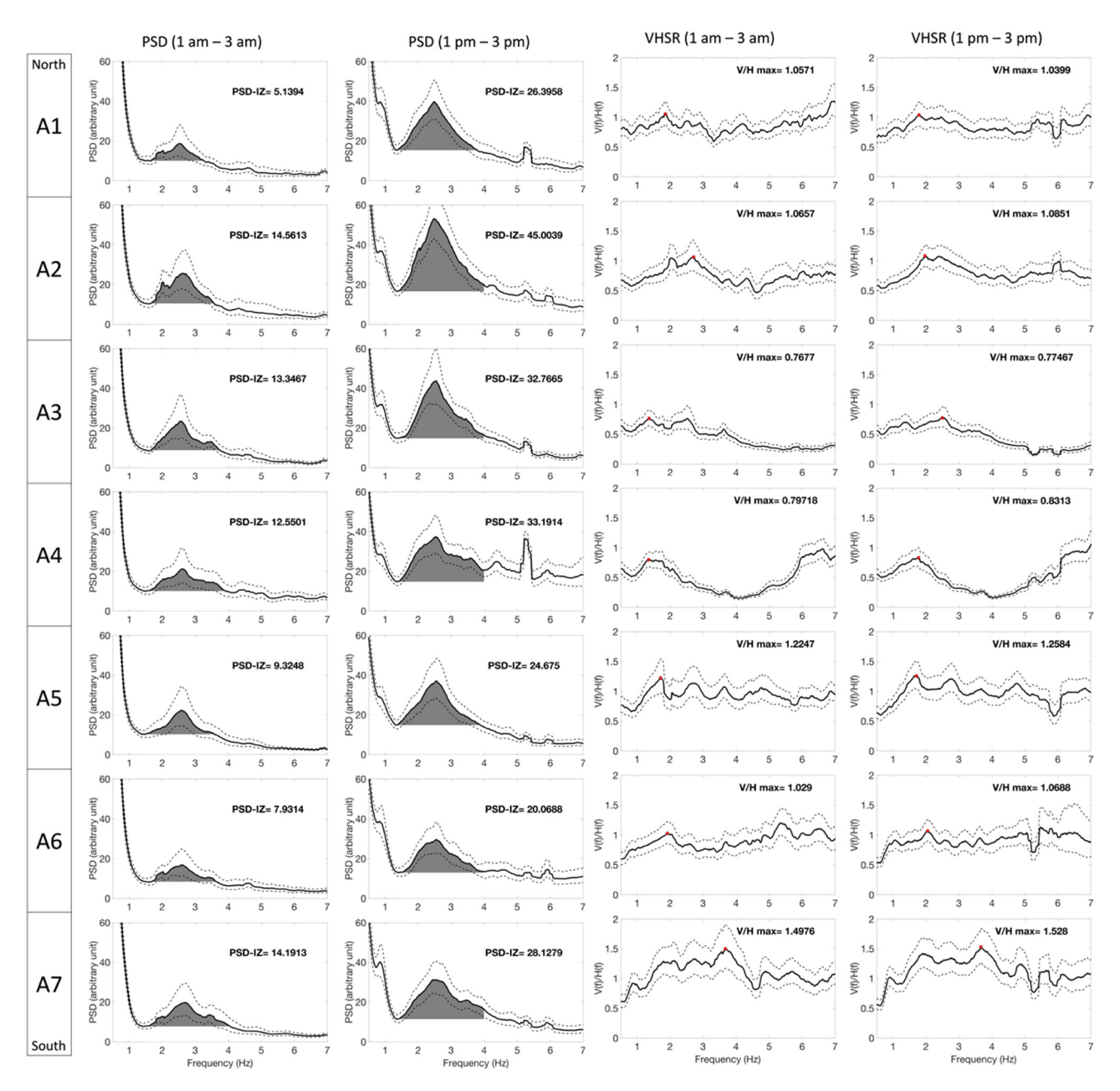


Figure 13: Spectral attributes obtained using 2 h of data during the night (1 am–3 am) and day (1 pm–3 pm); PSD and VHSR for seven stations at Line A. The black lines are the stacked spectra and their standard deviations. The gray areas represent PSD-IZ.

noises strengthen the anomalies is also proposed by several studies [6–8]. Although their amplifications are various, they significantly influence the quantification itself. For instance, strong amplitudes arise at station A2 during day 2. Therefore, we will obtain a significantly different quantification if we compare the PSD-IZ values between that day and other nights.

Nevertheless, the day and night variations are less significant in VHSR, especially between so-known hydrocarbon-related frequencies. Although transient interferences can also be observed at station A4 during day 2, they can be removed. Meanwhile, other signatures seem to have remained smooth over time. For instance, a strong VHSR ratio appears at station 7 between 1 and 6 Hz time after time. Moreover, it is well related to the stacked VHSR shown in Figure 9. This concludes that VHSR is stable over time, although it contributes less as a DHI.

Figure 13 illustrates the energy of anomalies we may obtain using the data recorded during quiet time at night and otherwise at noon. We calculated PSD and VHSR (as described in Section 3) for the 2-h duration of data in the night (between 1 am and 3 am) and the middle of the day (from 1 pm to 3 pm). As discussed, amplifications significantly contribute to the quantification of energy for PSD, while VHSR stays firm. This implies that a practical single temporal measurement for building a map of PSD, as suggested by Saenger et al. [5], may need to be revised in quantifications. Furthermore, confronting and comparing one site to another with a different measurement time without calibration becomes questionable. Therefore, normalization is a must to prevent misleading information in mapping the anomalies. We suggest conducting synchronized measurements using an array geometry for a few days. This may also be beneficial for the following ambient noise study to delineate structures and sediment layers in the study area [18,19].

5 Conclusions

We have shown the hydrocarbon-related spectral anomalies above a known oil reservoir area in Banyubang Field, Indonesia, represented by PSD-IZ and VHSR. The PSD-IZ shows a strong indication above the reservoir boundary, acting as a DHI. Although it does not necessarily relate to the reservoir thickness, the linear relationship between the PSD-IZ value and the high indication of a hydrocarbon reservoir can be emphasized. Meanwhile, VHSR gives a more complex pattern that may relate to the sediment thickness and contrasts around a reservoir area. Therefore, an independent interpretation of the VHSR ratio is impudent, while it may work as a complement for PSD-IZ.

Unfortunately, the spectral anomalies found at an observing station do not necessarily indicate the reservoir directly beneath it. The anticline structure may bend and scatter the ray path so it would not be vertically polarized. Due to the consequences of scattered waves, the observed anomalies could also be related to hydrocarbon indication near that site. Moreover, the distinguishment of dominant sources is essential to prevent any misinterpretation.

The continuation of hydrocarbon-related anomalies has been observed. Generally, the anomalies emerge continuously over time, especially for PSD. However, amplification of vertical PSD occurs during days and may mislead the quantification. Subsequently, mapping anomalies at different sites should require calibration to normalize the spectral amplitudes if the measurement times are unsynchronized. We also suggest remeasuring the interest area using an array geometry for a few days, at least after narrowing it from mapping.

Regardless, there is still a high possibility of LFPS applications in Indonesia. The important notes from this study should be taken that PSD-IZ plays a role as the main quantification of hydrocarbon-related energy, while VHSR acts to support it. Moreover, we also encourage conducting LFPS surveys in other fields to investigate the consistency of these findings.

Acknowledgements: We gratefully acknowledge Hibah Riset ITB 2018 awarded to A.P. for funding this research. We thank KSO Pertamina EP – Banyubang Blora Energi, for the permission to conduct the LFPS survey in Banyubang Field.

Author contributions: A.P., R.V.R., and A.D.N. conceived the study and contributed to the conception, analysis, and interpretation of data. A.L., B.S.P., and Y.M.H. designed and managed the LFPS survey. A.A. contributed to data analysis. N.W. and B.I.S. contributed to data interpretation. All authors contributed to the preparation of the manuscript. The data and material that support the findings of this study are available on request from the corresponding author, A.P., and R.V.R.

Conflict of interest: The authors declare that there is no conflict of interest.

Data availability statement: Data available on request from the author.

References

[1] Dangel S, Schaepman ME, Stoll EP, Carniel R, Barzandji O, Rode ED, et al. Phenomenology of tremor-like signals observed over hydrocarbon reservoirs. J Volcanol Geotherm Res. 2003;128:135–58.

- [2] Holzner R, Eschle P, Zurcher H, Lambert M, Graf R, Dangel S, et al. Applying microtremor analysis to identify hydrocarbon reservoirs. First Break. 2005;23:41-6.
- [3] Steiner B, Saenger EH, Schmalholz SM. Time reverse modeling of low-frequency microtremors: application to hydrocarbon reservoir localization. Geophys Res Lett. 2008;35:1-7.
- Lambert MA, Schmalholz SM, Saenger EH, Steiner B. Low-frequency microtremor anomalies at an oil and gas field in Voitsdorf, Austria. Geophys Prospect. 2009;57:393-411.
- Saenger EH, Schmalholz SM, Lambert M-A, Nguyen TT, Torres A, Metzger S, et al. A passive seismic survey over a gas field: analysis of low-frequency anomalies. Geophysics. 2009;74:029-40.
- Ali MY, Berteussen KA, Small J, Barkat B. Low-frequency passive seismic experiments in Abu Dhabi, United Arab Emirates: implications for hydrocarbon detection. Geophys Prospect. 2010:58:875-99.
- Hanssen B. Pitfalls in the analysis of low frequency passive seismic data. First Break. 2008;26:111-9.
- Ali MY, Berteussen KA, Small J, Barkat B, Pahlevi O. Results from a low frequency passive seismic experiment over an oilfield in Abu Dhabi. First Break. 2009;27:91-7.
- Ali MY, Barkat B, Berteussen KA, Small J. A low-frequency passive seismic array experiment over an: onshore oil field in Abu Dhabi, United Arab Emirates. Geophysics. 2013;78:B159-76.
- [10] Ali MY, Berteussen KA, Small J, Barkat B. A study of ambient noise over an onshore oil field in Abu Dhabi, United Arab Emirates. Bull Seismol Soc Am. 2010;100:392-401.
- [11] El Khoury C, Chauris H, Kazantsev A, Monteiller V. Rayleigh wave spectral distortions induced by an anticline structure. Geophys J Int. 2023;233:2067-83.
- [12] Kazantsev A, Chauris H, Dublanchet P, Huguet F. Rayleigh wave amplitude distortions above a reservoir: new insights from elastic modelling. Geophys | Int. 2019;217:1267-89.
- [13] Ramadhan D, Nugraha AD, Afnimar, Akbar MH, Mulyanagara G. Multi-attribute analysis of a low frequency passive seismic method for hydrocarbon indicator prospecting: case study in 'Cemara' Field, Cirebon, West Java, Indonesia. 37th Annual Convention & Exhibition Proceedings, Indonesian Petroleum Association; 2013.
- [14] Perbawa A, Yudhatama D, Arham MA. Application of low frequency passive seismic method for hydrocarbon detection in S Field, South Sumatra Basin. Proceedings HAGI-IAGI Joint Convention Medan; 2013.
- [15] Prabowo BS, Ry RV, Dian Nugraha A, Siska K. Hydrocarbon prospect derived from attributes analysis on low-frequency passive seismic

- survey: a case study from Kalimantan, Indonesia. IOP Conf Ser Earth Environ Sci. 62, 2017. p. 1-5.
- [16] Haris A, Riyanto A, Syahputra R, Gunawan A, Panguriseng MJ, Nuratmaja S, et al. Integrating a microtremor survey and time reverse modeling over a hydrocarbon reservoir: a case study of Majalengka field, West Java Basin, Indonesia. J Geophys Eng.
- Sudarmaji S, Nurcahya BE, Sugiantoro NR. Vertical to horizontal spectral ratio (VHSR) response of seismic wave propagation in a homogeneous elastic - poroelastic medium using the spectral finite element method. Indones J Appl Phys. 2021;11:95.
- Ry RV, Cummins PR, Hejrani B, Widiyantoro S. 3-D shallow shear velocity structure of the Jakarta Basin from transdimensional ambient noise tomography. Geophys J Int. 2023;234:1916-32.
- Setiawan A, Zulfakriza Z, Nugraha AD, Rosalia S, Priyono A, Widiyantoro S, et al. Delineation of sedimentary basin structure beneath the Banyumas Basin, Central Java, Indonesia, using ambient seismic noise tomography. Geosci Lett. 2021;8:1-15.
- [20] Soetantri B, Samuel L, Nayoan GAS. The geology of the oilfields in North East Java. Proceedings Indonesian Petroleum Association, 2nd Annual Convention; 1973.
- Pringgoprawiro H. Biostratigraphy and Paleogeography of the [21] North-East Java Basin, A new approach. Institut Teknologi Bandung; 1983.
- Jurkevics A. Polarization analysis of three component array data. Bull Seismol Soc Am. 1988;78:1725-34.
- Ry RV, Cummins PR, Widiyantoro S. Shallow shear-wave velocity beneath Jakarta, Indonesia revealed by body-wave polarization analysis. Geosciences. 2019;9:386.
- Ry RV, Septyana T, Widiyantoro S, Nugraha AD, Ardjuna A. Borehole [24] microseismic imaging of hydraulic fracturing: a pilot study on a coal bed methane reservoir in Indonesia. J Eng Technol Sci. 2019;51:251-71.
- [25] Suhascaryo N, Ariyanto B. Planning of casing design in AOV-1 well drilling, ANTARIS Field KSO Pertamina EP - Banyubang Blora Energi (BBE). PETRO J. 2021;2:71-85.
- [26] Vesnaver A, Da Col F, Jervis M, Kaka SI, Nieto D. On the use of microtremors for hydrocarbon detection. Geophys Prospect. 2014;62:897-909.
- [27] Nakamura Y. Method for dynamic characteristics estimation of subsurface using microtremor on the ground surface. Q Rep RTRI. 1989;30:25-33.
- [28] Nieto D, Baradello L, Kaka SI, Vesnaver A. Microtremors, a nearsurface phenomenon? J Seismic Explor. 2011;20:379-98.